A Novel Restricted Photoaffinity Spin-Labeled Non-Nucleoside ATP Analogue as a Covalently Attached Reporter Group of the Active Site of Myosin Subfragment 1†

Xiaoru Chen,[‡,§] Jean Grammer,[‡] J. David Lawson,[‡] Roger Cooke,[∥] Edward Pate,[⊥] and Ralph G. Yount*[,‡,@]

School of Molecular Biosciences, Department of Pure and Applied Mathematics, and Department of Chemistry, Washington State University, Pullman, Washington 99164, and Department of Biochemistry and Biophysics and CVRI, University of California, San Francisco, California 94143

Received September 25, 2001; Revised Manuscript Received December 6, 2001

ABSTRACT: The photoaffinity spin-labeled non-nucleoside ATP analogue, 2-(4-azido-2-nitrophenyl)amino-2,2-(1-oxyl-2,2,6,6-tetramethyl-4-piperidylidene)di(oxymethylene)ethyl triphosphate (SSL-NANTP), has been shown to be a substrate for skeletal mysoin subfragment 1 (S1) that can be photoincorporated at the active site of S1 [Chen, X., et al. (2000) *Bioconjugate Chem. 11*, 725−733]. Electron paramagnetic resonance spectroscopy shows that the probe undergoes restricted motion with respect to the protein. The parent compound, NANTP {2-[(4-azido-2-nitrophenyl)amino]ethyl triphosphate}, is specifically photoincorporated at Trp-130 on the amino-terminal 23 kDa tryptic fragment in rabbit skeletal myosin. Surprisingly, amino acid sequence analysis shows that SSL-NANTP is photoincorporated on the carboxy-terminal 20 kDa tryptic fragment at Lys-681 on the side opposite Trp-130 in the nucleotide pocket. This is the first direct evidence showing that this residue in the 20 kDa tryptic fragment is close enough to the active site to be photolabeled by trapped ATP analogues. After actin treatment in the presence of MgATP, SSL-NANDP-labeled myosin S1 had normal ATPase activity, indicating that photolabeling did not significantly alter the enzymatic properties of S1. Photoincorporated SSL-NANDP was bound inside the nucleotide site of S1, with an effective concentration of ∼20 mM as judged by the concentration of MgADP needed to displace it. Molecular dynamics simulations suggest that the ability of NANTP and SSL-NANTP to photolabel different sites results from different orientations of the phenyl ring in the active site. For SSL-NANTP, the *p*-azido group on the phenyl ring points toward Lys-681. For NANTP, it points in the opposite direction toward Trp-130.

The mechanism by which the motor protein, myosin, ATP, and actin interact to produce force and motion remains a fundamental, unresolved question in biology. The X-ray crystallographic structures of myosin subfragment 1 (S1)[1] and actin along with the derived structures of F-actin and of the docked actoS1 complex (*1*−*13*) have all provided significant insights into the molecular nature of contraction. Nonetheless, a detailed picture connecting these structures to the various steps in contraction remains to be determined.

The crystal structures show that S1 is comprised of a large globular region termed the catalytic domain that is connected via a converter region to a long α-helical neck. The neck is bound to two light chains that together are termed the regulatory, or light chain, domain. The catalytic domain contains sites for the binding of both actin and ATP. The nucleotide pocket is very open around the ribose and adenine ring portions of the nucleotide in all structures obtained to date, with only minimal hydrogen bonding from the protein to the adenine and ribose rings (reviewed in ref *14*). The triphosphates, on the other hand, are tightly encased in a narrow tunnel-like structure. This phosphate tube (P_i tube) (*15*) has three components: the P-loop and regions topologically similar to switch 1 and switch 2 in the G-proteins (*16*, *17*). Extensive protein−metal−ligand coordination is evident.

A popular hypothesis is that the interaction of myosin, ATP, and actin results in the myosin neck functioning as a rotating lever arm, driving filament sliding. Comparison of the motor domain structures of *Dictyostelium* myosin (MD_{dc}) structures with ADP·BeF_x and ADP·AlF_4, or ADP·Vi, at the active site (*2*, *3*) provided the first indications that lever arm motion could plausibly be related to conformational changes in the catalytic domain. The change from tetrahedral coordination around BeF_3 to a trigonal bipyramidal structure about Vi was accompanied by a partial closure of the 50 kDa cleft. There was a concomitant change in the position

† This work was supported by U.S. PHS Grants DK05195 (R.G.Y.), AR39643 (E.P.), and AR42895 (R.C.).

* To whom correspondence should be addressed. Telephone: (509) 335-3442. Fax: (509) 335-9688. E-mail: yount@wsu.edu.

‡ School of Molecular Biosciences, Washington State University.

§ Present address: Diazyme-General Atomics, P.O. Box 86508, San Diego, CA 92186.

∥ University of California.

⊥ Department of Pure and Applied Mathematics, Washington State University.

@ Department of Chemistry, Washington State University.

[1] Abbreviations: S1, myosin subfragment 1; P_i tube, phosphate tube; Dc, *Dictyostelium*; Vi, orthovanadate; SL-Bz_2ATP, 3′(2′)-*O*-4-[4-oxo-(4-amino-2,2,6,6-tetramethylpiperidinyloxy)-4-benzoyl]benzoyladenosine 5′-triphosphate; 4-amino-TEMPO, 4-amino-2,2,6,6-tetramethylpiperidinyloxy; NANTP and NANDP, 2-[(4-azido-2-nitrophenyl)-amino]ethyl tri- and diphosphate, respectively; SSL-NANTP, SSL-NANDP, and SSL-NANMP, 2-(4-azido-2-nitrophenyl)amino-2,2-(1-oxyl-2,2,6,6-tetramethyl-4-piperidylidene)-di(oxymethylene)ethyl tri-, di-, and monophosphate, respectively; DEAE, 2-(diethylamino)ethyl; SDS, sodium dodecyl sulfate; TPCK, *N*-tosyl-L-phenylalanine chloromethyl ketone; TLCK, tosyl lysine chloromethyl ketone; NTA, nitrilotriacetic acid; SSL-DNPEATP and SSL-DNPhAEDP, 2-(4-dinitrophenyl)amino-2,2-(1-oxyl-2,2,6,6-tetramethyl-4-piperidyl-idene) di-(oxymethylene)ethyl tri- and diphosphate, respectively; DNPhAETP, 2-[(2,4-dinitrophenyl)amino]ethyl triphosphate; SSL-NANDP−S1, SSL-NANDP covalently photoincorporated into rabbit skeletal S1; $S1_{sk}$, chicken fast skeletal muscle myosin subfragment 1; MD_{dc}, *D. discoideum* myosin motor domain; MD, molecular dynamics.

10.1021/bi0118411 CCC: $22.00
Published on Web 01/30/2002

of both switch 2 and an adjacent structurally conserved α-helix, termed the relay helix (*6*). This α-helix interacts with the SH1−SH2 helix and with the converter domain, which are seen to both rotate and translate. If the catalytic region were rigidly connected to the neck region (absent in the MD_{dc} structures), these structural changes would imply a large shift in the relative orientations of the neck and the catalytic domain (*18*, *19*). Subsequent S1 structures that retained the neck (*5*, *6*), electron microscopic (*20*, *21*), fluorescence (*22*−*24*), luminescence (*25*), and EPR spectroscopic (*26*, *27*) features provided additional support for nucleotide-dependent, myosin neck region rotations.

Major uncertainties remain, however, in correlating nucleotide-dependent orientational changes in the catalytic domain with neck movements. Crystal structures of different S1 isomers yield different neck orientations, despite identical ligands at the nucleotide site (*2*, *3*, *5*, *6*). There remains no clear explanation for why the nucleotide-free chicken S1 and MD_{dc}·ADP states (strong actin binding states, end of the power stroke) should be in the same class of crystal structures as MD_{dc}·ADP·BeF_3 and MD_{dc}·ATPγS (weakly binding states, beginning of the power stroke). The scallop S1·ADP structure (*6*) gives yet a totally different state with a melted SH1−SH2 helix and a dramatically rotated neck. It has likewise been shown that non-nucleoside triphosphate substrates can decouple hydrolysis from motility (*28*, *29*). Many of these substrates are hydrolyzed by myosin and actomyosin at rates even faster than that of ATP, without generating active tension or shortening. Thus, motions of switch 2 associated with changes in coordination between BeF_3 and Vi may be necessary for motility. However, the decouplers show that these changes are clearly not sufficient for motility. Other interactions at the nucleotide site must play pivotal roles. Even more puzzling are recent biochemical, fluorescence, biomechanical, and cross-linking studies that all indicate the P_i tube must open during the contractile cycle (*30*). A catalytic domain structure with an open P_i tube has not been seen by the S1 crystallographic studies.

Additional information about catalytic domain conformational changes is necessary to understand the working power stroke. Indeed, given a demonstrated, large conformational change at the P_i tube, and a postulated opening and closing of the large 50 kDa cleft in the catalytic domain (*10*−*12*, *18*, *19*), one cannot rule out catalytic domain orientational changes augmenting any lever arm motion. In addition, the fact that ATP is an effective substrate for contraction, but not GTP (*31*) or other decoupling substrates (*28*, *29*), points to the importance of possible conformational changes at the purine binding site. The need for additional reporter groups on the catalytic domain, particularly at the nucleotide site, motivates the studies reported here.

Electron paramagnetic resonance (EPR) spectroscopy has been a primary method used to monitor orientational changes in myosin (reviewed in ref *32*). Nucleotide site EPR probes on myosin or actomyosin in skinned fibers were originally limited to ATP and ADP analogues containing a spin probe moiety (*33*−*35*). A significant disadvantage to this approach has been the large, sharp spectral signal arising from unbound ATP and ADP analogues that masked the desired spectral components from probe bound to myosin or actomyosin. An alternative approach, which eliminated the signal from the unbound probe, was the synthesis of spin-labeled, photoaffinity ATP analogues. The first such analogue, SL-Bz_2ATP, contained a photoreactive dicarboxybenzophenone moiety esterified via one carboxyl group to the 3′(2′)-hydroxyls of ATP, and amidated via the second carboxyl group to the amine of 4-amino-TEMPO (*36*). The diphosphate probe could be stably trapped with vanadate at the nucleotide site and then covalently incorporated with high specificity and yield upon irradiation. The unincorporated probe could then be washed out, leaving only the reporter group covalently linked to the active site. Two different photoaffinity EPR probes, SL-NANTP and SSL-NANTP (Figure 1A), based upon the ATP analogue 2-[(4-azido-2-nitrophenyl)amino]-ethyl triphosphate (NANTP, Figure 1B) could similarly be stably trapped and photoincorporated into rabbit S1 in the diphosphate form (*37*). In the former, the spin moiety was attached to the nucleotide analogue via a methylamido linkage to the aminoethyl spacer. In the latter, attachment was via a more restrictive spiro linkage. All three analogues were substrates for S1 and actoS1, implying proper steric binding at the active site. Remarkably, SL-NANDP-, SSL-NANDP-, and SL-Bz_2ADP-photomodified S1 and actoS1 retained virtually normal enzymatic function after treatment with actin and MgATP (*36*, *37*). A disadvantage of SL-Bz_2-ADP and SL-NANDP was that the EPR spectra proved to be too mobile to provide orientational information at the active site following photoincorporation. This was presum-

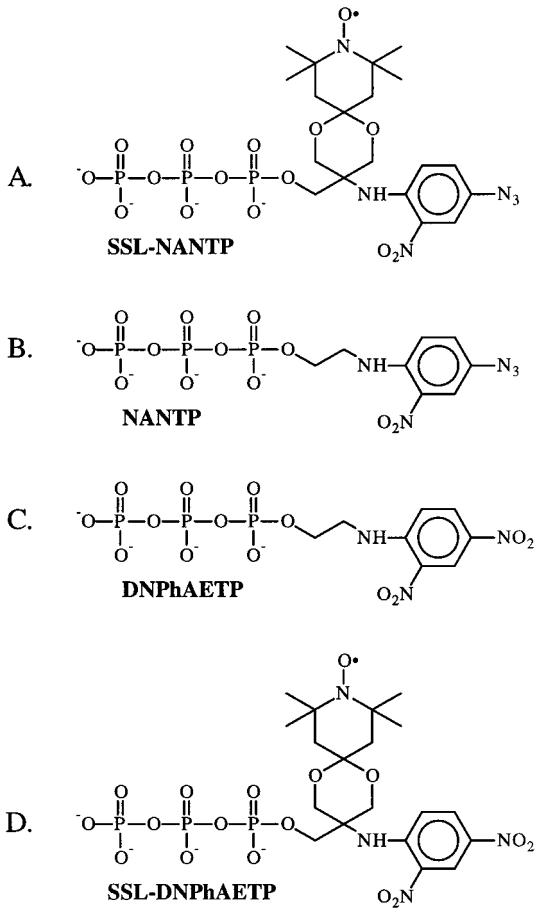

FIGURE 1: Structures of (A) SSL-NANTP; (B) the parent compound, NANTP; (C) DNPhAETP; and (D) SSL-DNPhAETP, which was used for molecular dynamics simulations. The differences between the NANTP- and DNPhAETP-based species are the replacements of the *p*-N_3 groups in the former with the *p*-NO_2 groups in the latter.

ably due to the single bond linkage of the spin-label moiety to the diphosphate species.

The EPR spectrum arising from S1 photoincorporated with SSL-NANDP instead showed a spectrum representing a spin probe undergoing restricted motion within a cone with a vertex angle of approximately 60° (*37*). The parent compound, NANTP, specifically photolabeled Trp-130 in the 23 kDa tryptic fragment of rabbit skeletal myosin (*38*), located at one edge of the entrance to the nucleotide pocket (*1*). SSL-NANDP instead is photoincorporated on the 20 kDa fragment, located on the opposite edge of the nucleotide pocket from Trp-130.

The ability of SSL-NANTP to yield immobilized EPR spectra when trapped at the active site, and to identify residues at the active site, suggests it as a potentially useful probe for actomyosin function. This motivated the further characterization of both the site of photoincorporation on rabbit S1 and the interaction of SSL-NANDP with S1. EPR spectroscopy showed that the probe could be displaced from the nucleotide site by ADP, giving a more mobile spectrum. The effective concentration of the covalently attached probe was surprisingly high (20 mM). Peptide mapping showed that SSL-NANTP is photoincorporated at Lys-681, located on the opposite side of the nucleotide pocket from Trp-130 in myosin crystal structures. This is the first definitive evidence from probes showing that this residue is sufficiently close to the nucleotide binding site to be photoincorporated by trapped ATP analogues. A molecular dynamics simulation of an SSL-NANTP analogue docked into a myosin crystal structure shows the plausibility of the observed photoincorporation of SSL-NANDP at Lys-681. It arises due to a dramatic rotation of the phenyl ring in the nucleotide pocket resulting from steric interference of the spin-label moiety.

MATERIALS AND METHODS

Materials. The sources of the chemicals that were used were as follows: BCA protein assay reagents from Pierce, sodium orthovanadate and Tris base from Fischer, chymotrypsin, TPCK-trypsin, TLCK, V8 protease, and Li_3ADP from Sigma, Ultimagold scintillation from Packard, and [^{32}P]-phosphoric acid from NEN.

Enzyme Preparations. Myosin was isolated from rabbit leg and back muscles as previously described (*39*) and stored in 50% glycerol at −20 °C. Chymotryptic S1 (115 000 g/mol) was prepared by a modification of the method of Okamoto and Sekine (*40*) as previously described (*41*), and stored in 50 mM Tris and 100 mM KCl at pH 8.0 and 4 °C (S1 buffer). F-Actin was purified from rabbit skeletal muscle as previously described (*42*).

Analytical Procedures. Protein concentrations were determined by the BCA protein assay or with Coomassie blue (Pierce) using unmodified S1 as the standard as previously described (*43*); $\epsilon_{280}^{1\%} = 7.5\ cm^{-1}$ (*44*). ATPase assays were performed as described previously (*45*), except that release of inorganic phosphate was assessed 2 and 8 min after the addition of S1 to the assay mixture. Actin-activated MgATPase assays were performed according to the previous method (*46*), and the detailed assay conditions are specified in the figure legends.

Vanadate Trapping and Photoincorporation of SSL-NANDP onto Rabbit Skeletal Myosin S1. SSL-NANTP and [^{32}P]SSL-NANDP were synthesized and characterized in our lab as reported previously (*37*). S1 (26.1 μM) was incubated with 2 mM $NiCl_2$, 0.1 mM [^{32}P]SSL-NANDP, and 1 mM Vi or an equivalent volume of S1 buffer (control) at 25 °C. After 40 min, EDTA (pH 8.0) and ATP were added to final concentrations of 20 and 5 mM, respectively, and the samples purified with Sephadex G-50 spin columns in S1 buffer. The purified S1·Ni·[^{32}P]SSL-NANDP·Vi complex was irradiated at 0 °C for 16 min using a Hanovia 450 W medium-pressure Hg lamp. To avoid photodamage and nonspecific labeling, a Pyrex filter and a Schott 408 filter were used to remove most of the radiation below 400 nm. To determine the amount of trapping, samples of the complex and the control before irradiation were counted by the liquid scintillation method and the protein concentrations were measured by using Coomassie blue. To determine the amount of covalent incorporation, known samples of the complex after irradiation were precipitated by addition of perchloric acid to a final concentration of 5% and centrifuged and the pellets were analyzed for radioactivity.

SDS−PAGE Analysis. Myosin S1 samples were analyzed by SDS−PAGE on 18 cm × 20 cm 12% gels according to the procedure of Laemmli (*47*). Protein bands were visualized by staining with a solution of Coomassie blue (0.07% Coomassie blue in a 5:5:1 methanol/water/acetic acid mixture). Gel strips containing the bands of interest were excised and placed in 20 mL glass vials. Ultimagold (Packard) (10 mL) was added, and the amount of radioactivity was determined.

Purification of the [^{32}P]SSL-NANDP-Labeled Tryptic 20 kDa Fragment. The S1·Ni·[^{32}P]SSL-NANDP·Vi complex (50 mg) was prepared and irradiated as described above. To form the characteristic 23, 50, and 20 kDa major tryptic fragments, the covalently labeled [^{32}P]SSL-NANDP−S1 complex was digested with trypsin (1:100, w/w) for 15 min at 25 °C and the reaction was quenched with soybean trypsin inhibitor (3:100, w/w). The sample was concentrated and the buffer exchanged with 50 mM Tris and 100 mM NaCl (pH 8.0 and 4 °C) by using a Centricon Plus-20 concentrator (Millipore). The major tryptic fragments were separated by preparative SDS gel electrophoresis on a Bio-Rad model 491 Prep Cell apparatus using a 4% acrylamide stacking gel and a 14% separating gel. The fragments were continuously eluted with 25 mM Tris, 192 mM glycine (pH 8.3), and 0.05% SDS during the electrophoresis, and 4.5 mL fractions were collected. To locate the 20 kDa fragment, aliquots of fractions were analyzed on 1 mm 12% SDS−PAGE (*47*) minigels (Novex). Fractions were also analyzed for radioactivity. The radioactive 20 kDa fragment was pooled, concentrated to 2 mL on a Centricon-Plus 20 concentrator, and precipitated with 2 volumes of cold ethanol. Following resuspension in water and a second precipitation with ethanol, the 20 kDa fragment (100 nmol total of which 15 nmol was [^{32}P]SSL-NANDP-labeled) was resuspended in 50 mM ammonium bicarbonate, 15 mM NaCl, 2 mM $CaCl_2$, and 2 M urea and digested by three additions of 1:100 (w/w) TPCK-trypsin at 0, 1, and 2 h. The digestion continued overnight at 25 °C. Initially, the tryptic digest was immediately separated via HPLC. In later experiments, the trypsin in the digest was quenched with TLCK and digested for an additional 18 h with V8 protease.

Use of Fe^{3+}NTA Columns To Purify Diphosphate-Containing Peptides. A Fe^{3+}NTA column (Qiagen) was used to purify the trypsin/V8 digest prior to HPLC separation. The column (2 mL) was prepared essentially as described by Neville et al. (*48*). Briefly, the column was rinsed with 0.1 M EDTA to remove any bound metal ions followed by sequential rinses with water (4 mL), 0.1 M acetic acid (6 mL), and freshly prepared and filtered 0.1 M $FeCl_3$ in 0.1 M acetic acid (10 mL) and rinsed thoroughly with 0.1 M acetic acid to remove any unbound Fe^{3+}. The digest was acidified with acetic acid to pH <4 and applied to the Fe^{3+}-loaded column, and the column was capped and mixed on a rotator for 2 h at room temperature. Following elution of the load volume, the column was rinsed sequentially with 0.1 M acetic acid (10 mL), water (4 mL), 50 mM Hepes (pH 7.2, 4 mL), 0.1% ammonium acetate (pH 8.0, 4 mL), 0.1% ammonium acetate, 4 M urea (pH 8.0, 2 mL), and 0.1% ammonium acetate (pH 8.0, 2 mL). Bound peptides were eluted with 0.1% ammonium acetate and 20 mM potassium phosphate (pH 9.5, 8 mL). Columns were rinsed with 0.1 M EDTA and either stored in EDTA or further rinsed with 0.1 M acetic acid and stored. All columns were run at room temperature.

HPLC Separations. Prior to HPLC separations, the digests were clarified by centrifugation on a Beckman microfuge followed by filtration through a 0.45 μm Acrodisc filter (Gelman). The peptides were separated by HPLC on a Brownlee C8 analytical column (220 mm × 4.6 mm) (Applied Biosystems) using a dual-pump Rainin system connected to a Waters 991 photodiode array detector. Fractions were analyzed for radioactivity in a Packard 1900CA apparatus either by Cherenkov counting or by using Ultima Gold (Packard) as the scintillant.

Peptide Sequence Analysis. Sequence analyses were performed on an ABI 475A pulse liquid sequencer (Applied Biosystems). Data were acquired and analyzed with the standard program Run 470-I (ABI).

EPR Spectra of SSL-NANDP-Photolabeled S1 (SSL-NANDP−S1). The SSL-NANDP−S1 complex was dialyzed into a buffer containing 0.18 M KOAc, 5 mM $Mg(OAc)_2$, 1 mM EGTA, 40 mM MOPS, and 200 μM P^1,P^5-diadenosine pentaphosphate (AP_5A) at pH 7.0 and room temperature (21−23 °C) (μ = 200 mM). The S1 was then concentrated in a Centricon tube to approximately 80 μM, mounted in a 50 μL glass capillary, and placed in the center of a TE_{011} EPR cavity. EPR measurements were performed with an ER/200D EPR spectrometer from IBM Instruments, Inc. (Danbury, CT). First-derivative, X-band spectra were recorded using 50 s, 12.5−13.0 mT wide sweeps with the following instrument settings: microwave power of 25 mW, gain of 1.0×10^5 to 1.0×10^6, center field of 347.8−348.0 mT, time constant of 200 ms, frequency of 9.3 GHz, and modulation of 0.2 mT at a frequency of 100 kHz. Each spectrum used in data analysis represents the average of 5−25 distinct sweeps from an individual experimental preparation.

For experiments involving titrations as a function of the concentration of MgADP ([MgADP]), the above S1-containing buffer was proportionally mixed with a buffer containing 1 mM EGTA, 50 mM $Mg(OAc)_2$, 50 mM Na_2ADP, 40 mM MOPS, and 200 μM AP_5A at pH 7 and room temperature (21−23 °C) (final concentrations, $[Mg^{2+}]$ = 5.1 mM, [MgADP] = 43 mM, μ = 200 mM). The concentrations of the various ionic species were calculated from standard binding constants as described previously (*28*). The concentrations of the various ionic species are not linear functions of the added components, and the use of proportional mixing to form buffers with intermediate MgADP concentrations resulted in ≤0.5% error in either the calculated MgADP concentration or ionic strength (*49*). This small error was ignored. In other experiments, 1 mM sodium orthovanadate (Vi) was added to an ADP-containing buffer as described above. For EPR experiments involving the untrapped SSL-NANDP·BeF_3 complex at the active site, 60 μM SSL-NANTP, 1 mM $BeCl_2$, and 8 mM NaF were added to the S1-containing buffer. The rigid limit, 7.16 ± 0.01 mT (two observations), was determined by freezing the S1·SSL-NANDP complex.

Molecular Dynamics Modeling. To better understand why SSL-NANTP photolabels Lys-681 rather than Trp-130, we carried out molecular dynamics (MD) modeling of analogues of SSL-NANTP and of rabbit S1. All structural modeling and visualization were performed on an SGI Indigo R4400 workstation using Biosym/MSI InsightII 3.0.0 software. No crystal structures exist for SSL-NANTP and rabbit skeletal myosin S1. As a substitute, we used the known structure of the NANTP analogue, DNPhAEDP·BeF_3, bound to the motor domain of *Dictyostelium discoideum* myosin (MD_{dc}) (*7*). DNPhAETP differs from NANTP only in having a *p*-NO_2 group in place of the *p*-N_3 group on the phenyl ring of NANTP (Figure 1B,C). The spiro ring and spin-label moiety were then added to create SSL-DNPhAETP (Figure 1D) using the Biosym/MSI Biopolymer module. This new compound was docked into the known MD_{dc}-Mg·DNPhAEDP·BeF_3 structure to give a structure with the spiro ring and spin probe pointing out into the solvent from the active site. MD_{dc} does not have the photolabeled tryptophan at the active site. Furthermore, although it is a conserved residue (*50*), Lys-681 in MD_{dc} is spatially replaced with Gln-662 due to an amino acid deletion in the MD_{dc} sequence. Therefore, we superimposed the known structure of chicken skeletal myosin ($S1_{sk}$) onto the MD_{dc}-Mg·DNPhAETP structure using a least-squares distance minimization of the C_α backbone of the P-loop motifs as previously described (*51*). The resulting $S1_{sk}$-Mg·SSL-DNPhAETP structure was then used for MD simulations. $S1_{sk}$ has both the active site Trp-131 (Trp-130 in rabbit myosin) and Lys-681 in locations spatially homologous to those in rabbit muscle.

The structure was further modified in the following ways before MD simulations were carried out. The indole nucleus of Trp-131 was rotated to be adjacent to the phenyl ring of SSL-DNPhAETP by rotating the C_α−C_β bond of Trp-131 by 110° and the C_β−C_γ bond by 30°. The indole nucleus is known to be photolabeled by both NANTP (*38*) and 2-N_3-ATP (*52*), but in the $S1_{sk}$ structure, it points away from the active site without the above rotations. The heavy chain was truncated at residue 784, and the light chains were deleted. Regions of $S1_{sk}$ not resolved in the crystal structure were not added. The amino and carboxyl termini were then capped with uncharged amino and carboxy groups. A subset of this model was then created that included the Mg·SSL-DNPhAETP species itself and all residues in $S1_{sk}$ within approximately 14 Å of the Mg·SSL-DNPhAETP species. Resolved waters within 10 Å of the DNPhAEDP molecule in the MD_{dc}·Mg·DNPhAEDP·BeF_3 structure were also

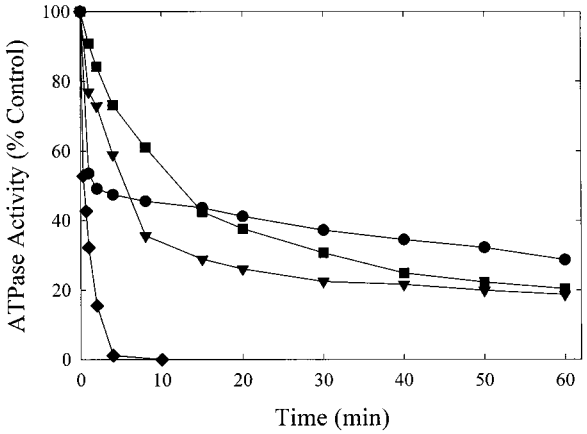

FIGURE 2: Inactivation of S1 by the SSL-NANDP·Vi or SSL-NANDP·AlF_4 complex. S1 was treated as described in Materials and Methods. (◆) S1 (18.6 μM) was incubated with 0.1 mM ADP, 2 mM $MgCl_2$, 5 mM NaF, and 1 mM $AlCl_3$ in S1 buffer. (▼) S1 (18.6 μM) was incubated with 0.1 mM SSL-NANTP, 2 mM $CoCl_2$, and 1 mM Vi in S1 buffer. (●) S1 (18.6 μM) was incubated with 0.1 mM SSL-NANTP, 2 mM $MgCl_2$, 5 mM NaF, and 1 mM $AlCl_3$ in S1 buffer. (■) S1 (18.6 μM) was incubated with 0.1 mM SL-NANTP, 2 mM $NiCl_2$, and 1 mM Vi in S1 buffer. At various times, reactions were quenched by addition of EDTA to a final concentration of 20 mM, and the NH_4^+-EDTA ATPase activity was measured.

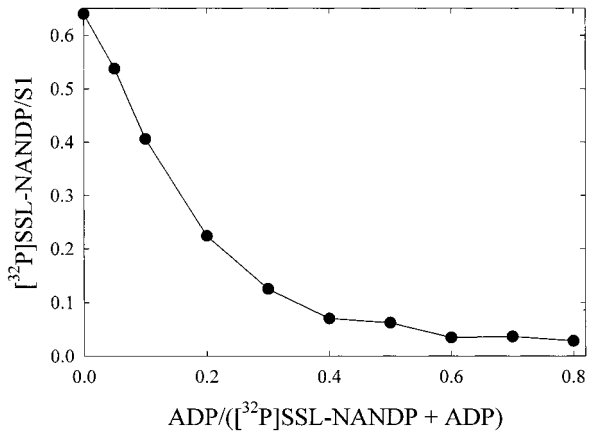

FIGURE 3: Competition of ADP and [^{32}P]SSL-NANDP for trapping on S1. S1 (17 μM) was inactivated by 1 mM vanadate in the presence of 2 mM $NiCl_2$, 85 μM [^{32}P]SSL-NANDP, and varying concentrations of ADP to give the indicated ADP/([^{32}P]SSL-NANDP + ADP) ratio. After 40 min at 25 °C, the reactions were quenched with EDTA (20 mM final concentration) and ATP (2.1 mM final concentration) and the samples purified with G-50 Sephadex spin columns. The amount of radioactivity and protein concentration were measured.

retained. This dynamic subset was then solvated with a 10 Å shell of explicit waters. A further 4 Å shell of waters was placed outside of the first shell, and the oxygens in this second shell were fixed to keep the inner dynamic waters from boiling off during the simulation. Protein and water parameters were assigned according to the AMBER force field (*53*). Mg^{2+} ion parameters were from Aqvist (*54*). SSL-DNPhAETP parameters were added using a custom parameter set based on AMBER CVFF potentials and ESFF charges (*55*). Force field parameters for the nucleotide analogue can be obtained from J. D. Lawson.

Minimizations and MD simulations were run with a 7.5 Å nonbonded cutoff and a 2.0 Å switching distance using Biosym/MSI Discover version 2.9.7. The dynamic protein subset and solvent were then minimized using 250 steps of steepest descents and 750 steps of conjugate gradients with the oxygens in the outer 4 Å shell of water fixed in place. The MD simulation was then initiated with the dynamic solvent and dynamic protein subsets free to move. The system was equilibrated by increasing the temperature from 0 to 300 K in 30 K steps. Each step was run for 2.5 ps. Trajectory data were recorded every 500 fs during the equilibration. Following the 300 K equilibration, the MD simulation then continued for 100 ps at 300 K with trajectory data recorded every 100 fs.

RESULTS

Trapping of SSL-NANDP at the Active Sites of Myosin S1. It has been shown previously that ADP and various ADP analogues can be trapped at the active site of skeletal, smooth, and scallop muscle myosin by treatment with divalent metal and vanadate (Vi), BeF_3, and AlF_4 (*41*, *56*−*61*). The phosphate analogues are known to replace the γ-phosphoryl group of ATP and its analogues, and form a stable transition state analogue of the S1·MgADP·P_i intermediate. Figure 2 shows the change of NH_4^+-EDTA ATPase activity that results from incubating S1 with SSL-NANTP, ATP and Vi (Ni^{2+} or Co^{2+}), or AlF_4 (Mg^{2+}). The rate of inactivation of SSL-NANDP with S1 was much slower than that of ADP. We were also unable to increase the percentage of trapping of SSL-NANDP onto S1 through addition of either more probe or more Vi. However, approximately 80% of the ATP binding sites were complexed with SSL-NANDP using Vi and Ni^{2+} (*37*). There was a parallel decrease in the NH_4^+-EDTA ATPase activity to a value ∼20% of that for untrapped myosin, indicating that SSL-NANTP is still an effective analogue of ATP.

Further evidence that SSL-NANDP was trapped at the active sites of S1 came from a trapping inhibition study. As seen in Figure 3, approximately 65% of ATP binding sites were effectively trapped with [^{32}P]SSL-NANDP in the absence of ADP, but the trapping percentage decreased with an increasing ratio of ADP to total substrate ([^{32}P]SSL-NANDP and ADP). Only ∼3% of the active sites were trapped with [^{32}P]SSL-NANDP in the presence of 80% ADP and 20% [^{32}P]SSL-NANDP. These results show that SSL-NANDP and ADP compete for the same binding site, but the affinity of SSL-NANDP was weaker than that of ADP.

Stability of the S1·Ni·SSL-NANDP·Vi and S1·Co·SSL-NANDP·Vi Trapped Complexes. To evaluate the stability of the trapped complexes, the NH_4^+-EDTA ATPase activities of the purified complexes were measured at various time points. The results (Figure 4) indicated that the half-life on ice was more than 1 day for the S1·Ni·SSL-NANDP·Vi complex, but only 5 h for the S1·Co·SSL-NANDP·Vi complex. The complex with Ni^{2+} and Vi was stable enough to allow it to be purified free of unbound probes, but the complex with Co^{2+} and Vi was not. Complexes with both Ni^{2+} and Vi and Co^{2+} and Vi were substantially less stable at room temperature.

Covalent Photoincorporation of Trapped SSL-NANDP into S1. Specificity of labeling is an important consideration in the photoincorporation of ATP analogues in myosin. It has been shown that trapping of nucleotide analogues prior to irradiation is essential for obtaining specific photolabeling

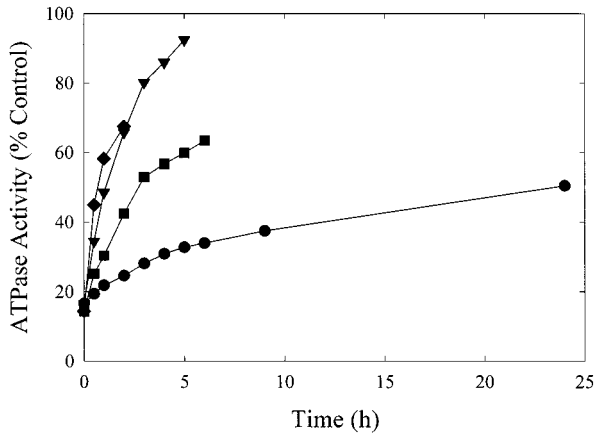

FIGURE 4: Stability of the S1·Co^{2+}·SSL-NANTP·Vi and S1·Ni^{2+}·SSL-NANTP·Vi trapped complexes. After S1 (17.6 μM), $CoCl_2$ or $NiCl_2$ (2 mM), SSL-NANTP (0.1 mM), and Vi (1 mM) in S1 buffer were incubated for 1 h at 25 °C, and EDTA and pyrophosphate were added to final concentrations of 20 and 5 mM, respectively. The trapped complex was purified with a G-50 column. The NH_4^+-EDTA ATPase activities were measured at various time points: (●) Ni−Vi, 4 °C; (▼) Ni−Vi, 25 °C; (■) Co−Vi, 4 °C; and (◆) Co−Vi, 25 °C.

Table 1: ATPase Activities (μmol of P_i mg^{-1} min^{-1}) of the SSL-NANDP−S1 Complex[a]

ATPase conditions	control S1	SSL-NANDP-labeled S1	% control
NH_4^+	19.0 ± 0.50	15.45 ± 0.45	81.3
Ca^{2+}	1.14 ± 0.10	1.11 ± 0.12	97.4
Mg^{2+}	0.055 ± 0.005	0.061 ± 0.006	110.9
Mg^{2+} with actin	5.68 ± 0.14	5.48 ± 0.05	96.5

[a] S1 was inactivated by 2 mM $NiCl_2$, 0.1 mM SSL-NANTP, and 1 mM Vi for 60 min at 25 °C. The trapped complex was purified and irradiated as described in Materials and Methods. Actin was used to release the free SSL-NANDP and Vi as described previously (*63*). The ATPase assays were performed at 25 °C under the following conditions: 44 mM Tris, 38 mM EDTA, 0.23 M KCl, 0.56 M NH_4Cl, 6.3 mM SSL-NANTP or ATP, and 0.10 μM S1 (pH 8.0) for NH_4^+-EDTA ATPase; 152 mM KCl, 15.2 mM $CaCl_2$, 152 mM Tris, 7.6 mM SSL-NANTP or ATP, and 0.90 μM S1 (pH 7.7) for Ca^{2+}ATPase; 10 mM Tris, 3 mM $MgCl_2$, 3 mM SSL-NANTP or ATP, and 1.0 μM S1 (pH 7.9) for Mg^{2+}ATPase; and 10 mM Tris, 3 mM $MgCl_2$, 3 mM SSL-NANTP or ATP, 0.20 μM S1, and 4.0−119 μM actin (pH 7.9) for actin-activated MgATPase.

of the active site of myosin (*38*, *52*, *62*). After incubation of S1 with [^{32}P]SSL-NANTP and Vi as described in Materials and Methods and subsequent removal of untrapped SSL-NANTP and Vi by gel centrifugation columns, the trapping efficiency was found to be high. More than 60% of the sites were trapped. After irradiation, it was found that approximately 15% of the active sites in S1 were covalently labeled (*37*). Here the Ni^{2+} was used as the metal to prevent vanadate-promoted photooxidation of myosin (*41*).

Enzymatic Activities of the Purified SSL-NANDP−S1 Complex. After irradiation, the protein solution was a mixture of covalently photolabeled S1, unmodified S1, and trapped but unmodified S1. Irradiated samples were treated with actin at a low ionic strength to release trapped Vi and noncovalently bound SSL-NANDP before adding excess ATP to dissociate S1 and photolabeled S1 from the actin. The samples were then centrifuged, and the supernatant was purified by gel filtration as described previously (*63*). The ATPase activities of the purified photolabeled S1 are given in Table 1. The Ca^{2+}ATPase, Mg^{2+}ATPase, and actin-activated MgATPase activities of the photolabeled S1 were fully recovered, but the NH_4^+-EDTA ATPase activity was ~80% recovered. These results indicated that divalent metals are needed to allow ATP to displace the covalently attached SSL-NANDP. Thus, the loss of NH_4^+-EDTA ATPase activity agreed roughly with the degree of photolabeling (13%).

Localization of [^{32}P]SSL-NANDP on Myosin S1. [^{32}P]SSL-NANDP was trapped by Vi and Ni^{2+} and subsequently photoincorporated onto S1 as described in Materials and Methods. The labeled S1 was analyzed by SDS−polyacrylamide gel electrophoresis to identify the labeled subunits. As shown previously, the radioactivity was only found in the 95 kDa myosin heavy chain (*37*). Neither the regulatory light chain nor the essential light chain was labeled. To localize the site of [^{32}P]SSL-NANDP covalent labeling within the heavy chain, photolabeled S1 was briefly digested with trypsin and analyzed on a 12% SDS gel. As in Chen et al. (*37*), the radioactivity analyses showed that essentially all of the photoincorporated [^{32}P]SSL-NANDP was found in the 20 kDa carboxyl-terminal tryptic fragment.

Purification of [^{32}P]SSL-NANDP-Labeled 20 kDa Fragments. Limited trypsin digestion of rabbit fast skeletal myosin yields three fragments: the amino-terminal 23 kDa fragment, the 50 kDa fragment, and the carboxy-terminal 20 kDa fragment. NANDP has previously been shown to photolabel Trp-130 on the 23 kDa fragment (38), and the homologous Arg-128 of scallop muscle (*60*). Instead, SSL-NANDP labeled the 20 kDa fragment. The following protocols were used to identify the peptide labeled with SSL-NANDP. To simplify the isolation of the labeled peptide, the labeled 20 kDa tryptic fragment was purified by preparative electrophoresis on a Bio-Rad Prep Cell prior to exhaustive trypsin digestion. The radioactive profile showed two major peaks of radioactivity (data not shown). The first peak (a doublet) eluted slightly before, and concomitant with, the dye front. It would be expected to contain free probe that had been trapped but not photoincorporated. The second peak of radioactivity corresponded to the 20 kDa fragment as shown by SDS−PAGE analysis, and accounted for approximately 75% of the covalent radioactivity that was loaded. There were no other radioactive peaks corresponding to the 23 and 50 kDa fragments. This result is in agreement with published data from analytical gel electrophoresis (*37*).

Isolation of the Labeled Peptide. The purified labeled 20 kDa fragment was digested by trypsin, and the resulting peptides were separated by HPLC as described in Materials and Methods. The labeled peptides were initially separated on an analytical C8 reversed phase column at neutral pH using a shallow (0.33%/min) gradient. As shown in Figure 5A, the labeled peptides eluted in a broad polymodal peak. Peptides eluting between 105 and 140 min were divided into three pools (A−C) as shown in Figure 5A. These peptides accounted for approximately 65% of the recovered radioactivity. Peptide pool A (fractions 105−113) was further purified on the same column at pH 2 using a 0.33%/min linear gradient of 0.11% TFA (solvent A) to 0.1%TFA and 60% CH_3CN (solvent B) as shown in Figure 5B. The labeled peptides eluted as a broad peak between 87 and 115 min that accounted for approximately 66% of the applied radioactivity. Two peptide pools were made [fractions 91−94 (A1) and 95−99 (A2)] and were submitted for sequence analysis. Peptide pool C from the initial HPLC separation (Figure 5A) was also purified in a similar manner (data not

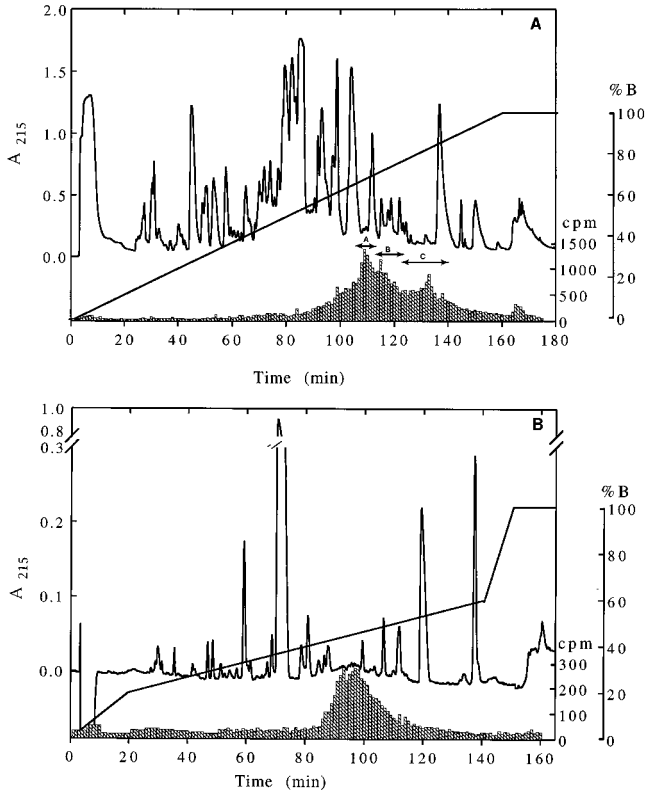

FIGURE 5: HPLC separation of a tryptic digest of the [^{32}P]SSL-NANDP-labeled 20 kDa tryptic fragment of S1. (A) S1 was photolabeled with [^{32}P]SSL-NANDP, and the labeled tryptic 20 kDa fragment was purified by preparative electrophoresis as described in Materials and Methods. Following exhaustive digestion with trypsin, the digest was separated by reversed phase HPLC on a Brownlee C8 analytical column equilibrated in 5 mM potassium phosphate (KP_i) at pH 6.9. The column was developed with a 0.33% linear gradient of KP_i to 65% CH_3CN/H_2O at a flow rate of 1 mL/min. Aliquots of each fraction (20 μL) were analyzed for radioactivity (shaded area), and three peptide pools were made (A−C) for further purification. (B) Peptide pool A (fractions 105−113) was further purified on the same column except the column was equilibrated in 0.11% TFA and developed with a 0.33%/min linear gradient of 0.1% TFA and 60% CH_3CN. An aliquot (20 μL) from each fraction was analyzed for radioactivity (shaded area). Two peptide pools were made [fractions 91−94 (A1) and 95−99 (A2)] and were submitted for sequence analysis.

shown) and sequenced. Attempts to improve the HPLC separations by removal of the phosphates from SSL-NANTP-labeled peptides by alkaline *Escherichia coli* phosphatase treatment were unsuccessful.

Amino Acid Sequence Analysis. The sequence data for the three peptides analyzed from this preparation are shown in Table 2. The sequence for all three (A1, A2, and C1) was found to be (C_{674})-I-I-P-N-E-T-(K_{681})-T-P-G-A-M-E-(H_{688})-E-L-V-L_{692}. The sequence analysis was terminated after 19 cycles, but the peptide likely continues onto the next tryptic site, Arg-695. Two lines of evidence support Lys-681 as being the site of photomodification. First, this sequence contains an internal lysine that would normally be expected to be cleaved by trypsin. Modification of this lysine would be expected to inhibit the cleavage by trypsin at this site. Second, the sequence yield of lysine drops to very low levels, whereas the yields of the next amino acids return to the expected levels. Again, modification of lysine would alter its chromatographic properties during sequence analysis. We attempted to monitor the amount of radioactivity released at each cycle but were unable to detect any. It was found that essentially all the radioactivity had been retained on the positively charged Polybrene-coated filter as would be expected for the negatively charged phosphates of the [^{32}P]SSL-NANDP attached to the lysine side chain. The yields for His-688 are also low, indicating that it may also be labeled. However, inspection of the crystal structures of all previously determined complexes of NANTP-based analogues with S1 (six total) shows that the homologous residue (Glu-668) is more than 16 Å from the phenyl ring in all S1 complexes (*7*), and separated by the bulk of the loop in the 20 kDa fragment that includes Lys-681. Hence, it is unlikely to be labeled.

Table 2: Sequence Analysis of the Major Photolabeled Peptides from the [^{32}P]SSL-NANDP−S1 Complex

		amino acid yield (pmol)[a]					
amino acid	cycle	A1	A2	C1	I	II	III
C	1	–	–	–	–	–	–
I	2	125	190	156	254	167	160
I	3	228	361	142	482	286	347
P	4	116	178	109	269	187	197
N	5	81	86	58	156	119	135
E	6	45	88	92	113	47	97
T	7	40	68	51	64	59	63
K	8	7	8	8	9	5	5
T	9	40	48	33	77	44	65
P	10	33	36	40	67	68	53
G	11	30	43	101	79	45	84
A	12	44	53	32	56	24	43
M	13	38	29	27	34	23	25
E	14	11	23	25	22	22	21
H	15	5	3	–	2	2	–
E	16	13	31	29	28	30	25
L	17	26	31	21	3	6	14
V	18	24	16	18	3	3	NA
L	19	26	45	22	4	5	NA

[a] Picomole yield of PTH amino acids. The sequence of the isolated, labeled peptides from the photoincorporated [^{32}P]SSL-NANDP−S1 complex is Cys_{674}-Ile-Ile-Pro-Asn-Glu_{679}-Thr-Lys_{681}-Thr-Pro-Gly-Ala-Met-Glu_{687}-His_{688}-Glu-Leu-Val-Leu_{692}.

Isolation of Labeled Peptides following Purification by Immobilized Metal Ion Affinity Chromatography on an Fe^{3+}NTA Column. The samples submitted for sequence analysis contained small amounts of two to three other unidentified peptides. Although the C_{674}−L_{692} peptide was the major sequence in all the samples that were submitted, an attempt was made to obtain purer peptides. Again, the labeled 20 kDa tryptic fragment was first separated by preparative electrophoresis as described in Materials and Methods and then digested with trypsin. The trypsin in the digest was quenched with TLCK, and V8 protease was added to cleave at glutamic acids. The digest was applied to an Fe^{3+}NTA column as described in Materials and Methods. All radioactivity was retained on the column until elution with 0.1% ammonium acetate and 20 mM potassium phosphate (pH 9.5) (data not shown) was carried out. The eluted peptides were separated by reversed phase HPLC as described in the legend of Figure 5B except that the column was developed with a 1%/min gradient (Figure 6). From the chromatogram, it is clear that most peptides were not retained on the Fe^{3+}NTA column. The labeled peptides eluted as a broad bimodal peak between 44 and 70 min and were split into three peptide pools (I−III) which were analyzed for amino acid sequence. The Fe^{3+}NTA column flow through and initial wash was also analyzed by HPLC in a similar manner and was found to have a very complex composition

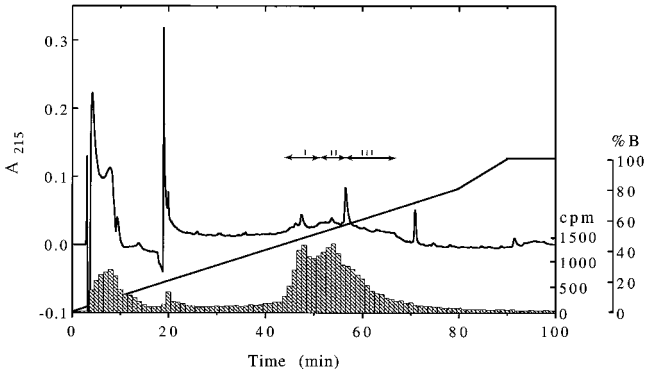

FIGURE 6: HPLC separation of a tryptic/V8 protease digest of the [^{32}P]SSL-NANDP-labeled 20 kDa tryptic fragment of S1 purified on an Fe^{3+}NTA column. S1 was photolabeled with [^{32}P]SSL-NANDP, and the labeled tryptic 20 kDa fragment was purified by preparative electrophoresis as described in Materials and Methods. Following sequential digestion with trypsin and protease V8, the digest was loaded on a 2 mL Fe^{3+}NTA column, washed, and eluted as described in Materials and Methods. The purified, labeled peptides were separated by reversed phase HPLC as described in the legend of Figure 5B except the gradient was 1%/min. Fractions were counted by Cherenkov counting (shaded area), and three peptide pools (I−III) were collected and submitted for sequence analysis.

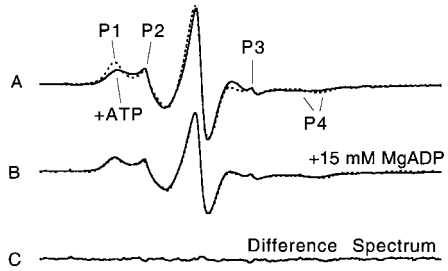

FIGURE 7: (A) EPR spectra of the S1−SSL-NANDP complex in the absence (- - -) and presence of 5 mM MgATP (—). (B) EPR spectrum of the S1−SSL-NANDP complex with 15 mM MgADP added (—). The dashed line is the least-squares fit assuming the spectrum in the presence of MgADP can be expressed as a linear combination of the two spectra in panel A. (C) Difference spectrum from the two spectra in panel B. All spectra are 12.7 mT wide.

as would be expected for a total digest of the 20 kDa fragment (data not shown). As shown in Table 2, the sequences of I, II, and III agreed with the data shown for the first three peptides sequenced except that it appears that V8 protease cleaved at Glu-689 for peptides I and II. Interestingly, it is apparent that V8 protease did not cleave at Glu-679. If Lys-681 is modified, it is likely that this could inhibit cleavage at this glutamate.

EPR Spectroscopy of the SSL-NANDP−S1 Complex. EPR spectroscopy can provide additional characterization of the photoincorporated probe. Figure 7A shows the EPR spectra obtained from the SSL-NANDP−S1 complex in the absence (- - -) and presence of 5 mM MgATP (—). The low-field to high-field splitting between P1 and P4 is a measure of the degree to which the probe is immobilized with respect to the protein. The greater this splitting, the more immobilized the probe. For the SSL-NANDP−S1 complex, the value for this splitting was 6.50 ± 0.02 mT (seven observations), comparable to the value obtained previously (*37*). The observed splitting shown in Figure 7 can be modeled by rapid motion of the probe within a cone with a vertex angle of 58° (*64*). The spectral component, P3 in Figure 7A, represents a small fraction of SSL-NANDP probes (<10%) which are covalently attached to S1 but highly mobile with respect to the protein. When 5 mM ATP is added to the S1 buffer (—), the peaks at P1 and P4 become broader and there is a decease in the level of high-field to low-field splitting, indicating a greater degree of angular mobility of the probe with respect to the protein. Increasing the MgATP concentration to 10 mM did not result in any additional change in the spectrum.

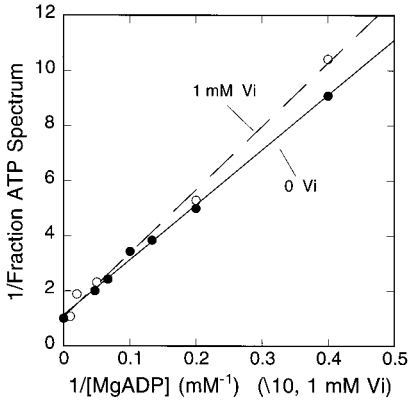

FIGURE 8: Double-reciprocal plot of the MgATP spectral component (Figure 7) in the EPR spectra obtained as a function of the concentration of MgADP for the S1−SSL-NANDP complex (●). The least-squares linear fit (− − −) defines an effective concentration of the photoincorporated probe of 17.3 mM. In the presence of added 1 mM Vi (○), the MgADP concentration required to give a 50/50 mixture of the two spectral components decreases by a factor of approximately 10. The values on the horizontal axis should be multiplied by 10 for experiments in the presence of 1 mM Vi.

Is the Covalently Attached Probe Bound in the Nucleotide Site? Upon addition of 15 mM MgADP to the SSL-NANDP−S1 complex, the spectrum that was obtained [Figure 7B (—)] appeared to be intermediate between the two spectra of Figure 7A. Analysis showed that the spectra obtained in the presence of added MgADP could in fact be represented as a proportionally weighted, linear sum of the two spectral components in Figure 7A. The fitted spectrum is shown as the dashed line in Figure 7B, and the difference between the two spectra from Figure 7B is given in Figure 7C, showing an excellent fit. The proportional linear combination for Figure 7B is 41% of the spectrum taken in the presence of MgATP in Figure 6A, and 49% of the dashed spectrum in Figure 6A. Using varying concentrations of added MgADP, Figure 8 shows a linear double-reciprocal plot of 1/[fraction of the ATP spectrum] [i.e., Figure 7A (—)] versus 1/[MgADP]. Using ATPase as the reporter signal, both previous studies with photoincorporated ϵBz_2ADP (*63*) and the studies reported here have implied that MgATP easily competes with covalently bound photoprobes at the nucleotide site. If we take the solid spectrum in Figure 7A to represent probes that are not in the nucleotide site, and the dashed spectrum to represent probes that are in the nucleotide site, the least-squares double-reciprocal plot (—, ●) in Figure 8 defines an effective concentration for the covalently attached probe of 17.3 mM for binding to the nucleotide site. This is only a factor of ∼2 higher than the effective concentration of 8 mM obtained for ϵBz_2ADP (*63*). When an identical decomposition of the spectra obtained at varying MgATP concentrations was carried out in the additional presence of 1 mM Vi, a linear double-reciprocal plot (Figure

8, − − −, ○) was obtained, but showing an approximately 10-fold decrease in the MgADP concentration required to produce a spectral shift comparable to that in the absence of added Vi. This decrease is to be expected because the MgADP·Vi species traps much more effectively at the S1 nucleotide site than does the SSL-NANDP·Vi species.

Due to probe mobility, we have previously been unable to determine whether an EPR spin probe that was covalently attached at the nucleotide site would bind in a stereospecific fashion inside the nucleotide pocket (*36*, *37*). Analysis of a three-state kinetic scheme including (1) the covalently attached photoprobe bound in the nucleotide pocket, (2) the covalently attached photoprobe out of the nucleotide pocket, and (3) the covalently attached photoprobe out of the nucleotide pocket with MgADP instead bound in the nucleotide pocket shows that a linear double-reciprocal plot is to be anticipated if the fraction of probes in state 2 is small (<10%) in the absence of added ADP. The spectra of Figure 7A are consistent with this approximation. Thus, both the linearity of the double-reciprocal plots and the alteration in affinity as a function of added Vi both argue that the SSL-NANDP−S1 spectrum of Figure 7A (- - -) represents probes that are bound inside the nucleotide site of S1. The solid spectrum in Figure 7A represents probes that are covalently attached to Lys-681, but have been displaced from the nucleotide site.

Is the Steric Binding of the Covalently Attached Probe in the Nucleotide Pocket Comparable to That of the Noncovalently Bound Photoprobe? Biochemical and spectroscopic data indicate that covalently attached SSL-NANDP can be bound in the nucleotide site. When bound in the active site, photoincorporated SSL-NANDP would be expected to be coordinated by the phosphates at one end of the analogue and by the linkage to Lys-681 at the phenyl ring end. Does the potential straining of the phosphate bonds by the lysine attachment significantly perturb the steric binding of the covalently attached analogue in the nucleotide pocket when compared to SSL-NANDP not covalently attached to S1? Does the covalently attached photoprobe have the correct steric binding? As previously noted, a difficulty in using EPR spectroscopy to monitor the binding of ATP analogues containing spin probe moieties to S1 is the large peaks in the spectra that result from the presence of unbound probe. These overlap with the low-field and high-field immobilized spectral components. The SSL-NANDP·BeF_3 complex binds more tightly to S1 than to SSL-NANDP, allowing us to virtually eliminate any EPR signal from the probe free in solution. Thus, we found that this analogue provided a better comparison for covalently and noncovalently attached EPR probe. Results are given in Figure 9. The dashed spectrum is from the covalently attached probe in the SSL-NANDP·BeF_3 state. The solid spectrum is from the probe bound in the SSL-NANDP·BeF_3 state but not covalently photoincorporated. The important observation is that the low-field to high-field splitting (P1−P5) is unchanged between the two spectra. The only difference between the spectra is that the spectrum from the photoincorporated probe shows a small (approximately 10%) increase in mobility. These results suggest the spin probes are equally immobilized in both preparations but not necessarily in the same position. The peaks at P2 and P4 in the solid spectrum are from the residual, untrapped SSL-NANDP free in solution, showing the dramatic reduction that was obtained with beryllium fluoride, enhancing resolution of the spectra. Virtually all the SSL-NANDP was trapped at the active site. We conclude that the additional strain on binding from simultaneous attachment to Lys-681 when the photoincorporated probe is bound in the nucleotide pocket does not significantly perturb the bound state. This conclusion would appear to place constraints on the distance from the nucleotide pocket to Lys-681.

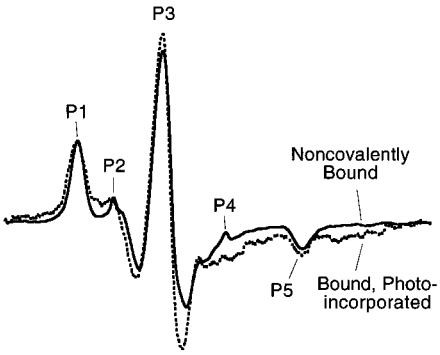

FIGURE 9: EPR spectrum of the SSL-NANDP·BeF_3 complex bound to S1 (—) and the EPR spectrum of SSL-NANDP covalently photoincorporated into S1 in the SSL-NANDP·BeF_3 complex (- - -). The spectra are 12.5 mT wide.

DISCUSSION

We have previously shown that the photoaffinity ATP analogue, EPR spin probe, SSL-NANDP, can photolabel the 20 kDa tryptic fragment of rabbit fast skeletal muscle myosin S1 (*37*). This was an unanticipated result in that the parent species, NANTP, specifically photolabels Trp-130 in the 23 kDa fragment. These two proteolytic fragments form opposite sides of the active site. In the work presented here, we have further characterized the interaction of SSL-NANDP with rabbit S1. We identify Lys-681 as the site of photoincorporation and use kinetic measurements and EPR spectroscopy to show that the photoincorporated probe binds in the nucleotide site with an effective concentration of 20 mM.

Trapping of SSL-NANDP at the active site of myosin is crucial to ensuring that photoincorporation on myosin is specific. There are several methods of trapping ADP or ADP analogues at the active site of myosin. The most useful methods involve forming stable complexes with divalent metal ions and phosphate analogues (*41*, *56*−*61*). Generally, complexes formed by these methods are stable at 0 °C and can be purified free of extraneous photoaffinity analogues prior to irradiation. Previous studies showed that NANDP can be stably trapped at the active site by forming complexes with Vi (*60*), and also by cross-linking SH1 and SH2 (*62*). Here we initially tried to use Vi and Co^{2+} to trap SSL-NANDP on S1. Unexpectedly, the S1·Co·SSL-NANDP·Vi complex was very unstable either on ice or at room temperature (Figure 3). We therefore tested other trapping reagents. Both AlF_4 and BeF_3 could trap SSL-NANDP at the active site with Mg^{2+}, and the complexes were stable. However, we were unable to completely remove untrapped [^{32}P]SSL-NANDP by gel filtration under these conditions. These results demonstrated that SSL-NANDP appears to bind tightly on a surface of S1 in the presence of Al^{3+} and Be^{2+}. We finally found that SSL-NANDP could be stably trapped with Vi if Co^{2+} was replaced with Ni^{2+}. The half-life of the S1·Ni·SSL-NANDP·Vi complex at 0 °C was more than 1

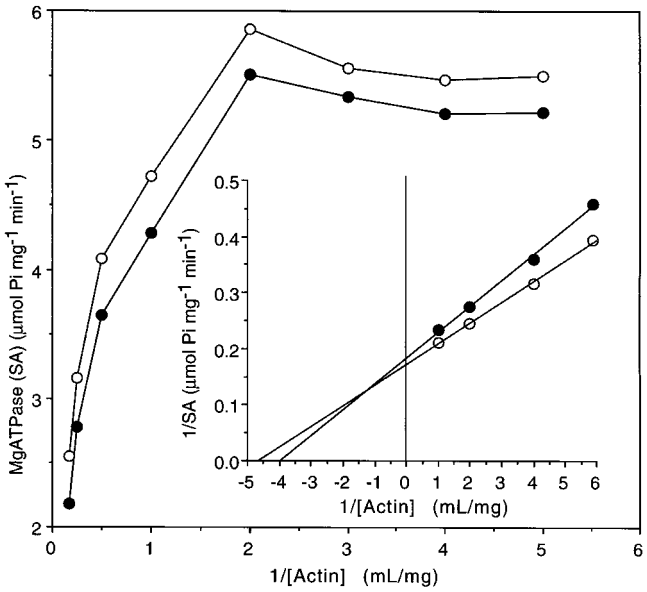

FIGURE 10: Actin-activated MgATPase activities of S1 (○) and the photolabeled SSL-NANDP−S1 complex (●) vs actin concentration. The amount of hydrolyzed P_i was measured by reading OD_{550} as described previously (*46*). ATPase activities at various actin concentrations were obtained by plotting OD_{550} data vs time. The inset gives least-squares linear, double-reciprocal plots for determining the values of V_{max} and K_m.

day (Figure 3), and under these conditions, the untrapped SSL-NANDP could be removed by gel filtration.

Previous results (*37*) demonstrated that a residue(s) in the 20 kDa fragment was the major site of photolabeling. Studies on isolated labeled peptides indicated that Lys-681 was specifically labeled, and no other labeled residues were detected (Table 2). The crystal structure of chicken skeletal S1 showed that Lys-681 was at the edge of the entrance to the ATP binding pocket (state 1), indicating that the labeling of Lys-681 was reasonable. This conclusion was consistent with the previous observation that mant-8-N_3-ADP·AlF_4^- (*65*) also photolabeled the 20 kDa tryptic fragment of rabbit skeletal S1. However, in this previous study, the labeled residue was not identified, but was localized to the Leu-660−Lys-702 peptide, which contained Lys-681.

Previous work has shown that rabbit skeletal myosin S1 could be specifically labeled at Trp-130 by the ATP photoaffinity analogues 2-N_3-ATP and NANTP, and at Ser-324 by Bz_2ATP. The labeling did not alter the actin-activated MgATPase activity of photolabeled S1 (*63*). The ATPase of SSL-NANDP-photolabeled S1 was likewise unaltered in the presence of Ca^{2+}, Mg^{2+}, or actin and Mg^{2+}, although there was a slight decrease in the NH_4^+-EDTA ATPase activity (Table 1). The study on the actin-activated MgATPase activity also showed that the affinity of the SSL-NANDP−S1 complex for actin ($K_m = 5.9 \times 10^{-6}$ M^{-1}) was similar to that of native S1 ($K_m = 5.2 \times 10^{-6}$ M^{-1}) (Figure 10).

EPR studies on the SSL-NANDP−S1 complex provided further support for the covalently attached probe binding at the nucleotide pocket. Competition experiments with MgADP and the MgADP·Vi complex showed a quantifiable spectral shift, consistent with the more immobilized component in the EPR spectrum arising from the photoincorporated probe bound in the nucleotide pocket. This is the first time it has been possible to conclusively demonstrate a change in the

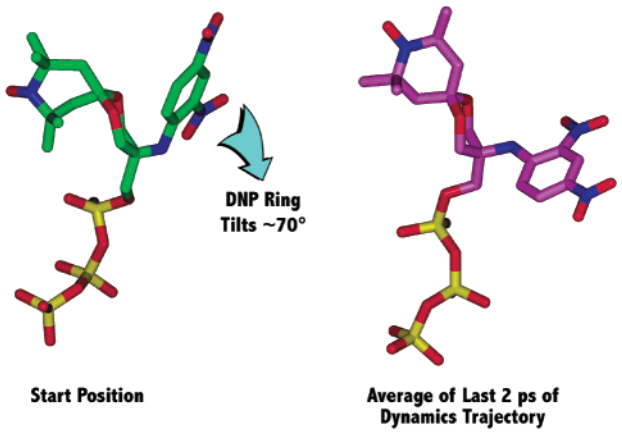

FIGURE 11: During the simulation, the phenyl ring of the docked SSL-DNPhAETP rotates by approximately 70° relative to its initial conformation.

EPR spectrum from a photoprobe that is in or out of the nucleotide pocket. Previous probes, not containing the restricted spiro ring attachment of the spin probe, have been too mobile for such resolution (*36*, *37*). Furthermore, the photoincorporated probe had a high effective concentration of almost 20 mM. Covalent attachment to Lys-681 did not substantively perturb the EPR spectrum from that of the noncovalently attached probe, again demonstrating proper steric binding in the nucleotide pocket of the photoincorporated probe. Further evidence that SSL-NANDP specifically occupied the ATP binding site was shown by a competition study in which ADP was able to inhibit formation of the trapped S1·Ni·[^{32}P]SSL-NANDP·Vi complex (Figure 2).

Molecular Dynamics Simulation of SSL-NANTP in the Nucleotide Pocket Explains Why Lys-681 Is Photolabeled Instead of Trp-130. As described in Materials and Methods, chicken skeletal S1 is the only crystal structure containing both the photolabeled lysine and tryptophan residues in locations spatially analogous to those in rabbit skeletal S1. MD simulations provide a powerful tool for evaluating the stability of accessible conformations of a ligand bound to a protein. Thus, we use MD simulations of chicken S1 with docked SSL-DNPhAETP to examine the temporal and spatial proximity of the photoaffinity analogue to the amino acid residues in question.

SSL-NANTP has a *p*-N_3 group on the phenyl ring, and N_2 is the leaving group in the photolabeling reaction. Thus, in our simulations, the distance from Lys-681 and Trp-131 to the nitrogen in the *p*-NO_2 group of SSL-DNPhAETP is the quantity of interest. The docked, energy-minimized structure that serves as the initial condition for our simulations provides no insight into the mechanism of photolabeling. The distance from the *p*-NO_2 nitrogen to N_ζ of Lys-681 is 7.3 Å in the initial structure, too far for obvious photolabeling. In contrast, the distance to the $C_{\epsilon 2}$ atom of Trp-131 (the distal carbon that join the five-membered and six-membered rings) is much shorter, only 4.5 Å. However, the movement of the phenyl ring of SSL-DNPhAETP during the MD simulation explains our experimental observation. Figure 11 shows the initial and final positions of the phenyl ring of SSL-DNPhAETP. In the initial location, taken from the previously determined (*7*) MD_{dc}·Mg·DNPEADP·BeF_3 crystal structure (green phenyl ring, left panel), the *p*-NO_2 group points toward Trp-131, as expected if it is the residue

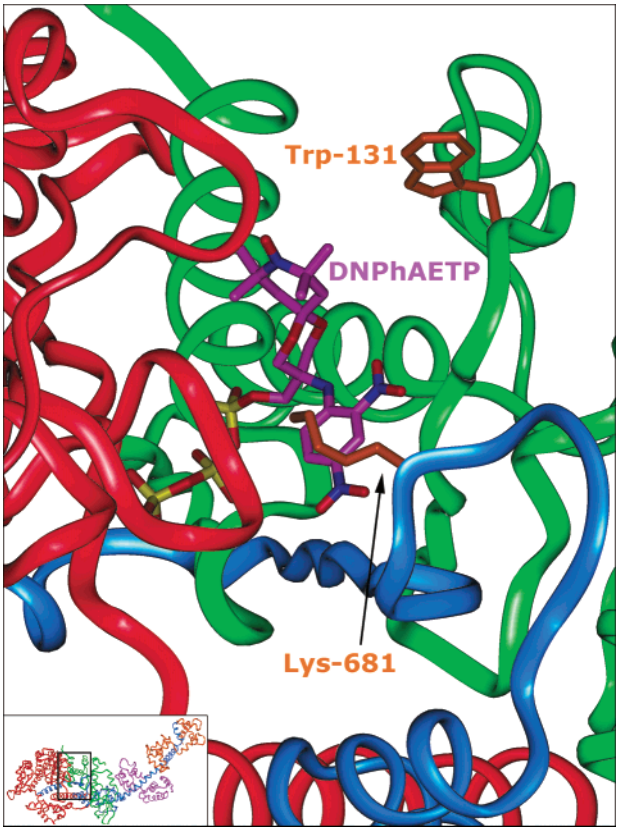

FIGURE 12: Position of Lys-681 relative to the Mg·SSL-DNPEATP complex modeled into the structure of chicken skeletal myosin S1 (*1*) after 70 ps of MD. The 50, 23, and 20 kDa tryptic fragments are shown in red, green, and blue, respectively. SSL-DNPEATP is rendered as a stick figure with purple carbons and yellow phosphates. The side chain of Lys-681 (stick figure in orange) projects away from the 20 kDa backbone toward the nucleotide binding cleft of the phenyl ring of the analogue, which has rotated away from Trp-131 (orange, top right). The inset shows the relative orientation of the S1 molecule in this view.

to be photolabeled. During the MD simulation, the phenyl ring tilts approximately 70°, adopting a very different conformation in which the *p*-NO_2 group (purple ring, right panel) is now oriented toward Lys-681. Figure 12 shows the final orientation of SSL-DNPhAETP in detail. The spin moiety is in the center, with the purple *p*-NO_2 phenyl ring group pointing toward Lys-681 (orange), and away from Trp-131 (orange, upper right). This change of orientation is better quantitated in Figure 13 which gives the simulated distance between the *p*-NO_2 nitrogen and the N_ζ atom of Lys-681 as a function of time. During the first 5 ps of the simulation, the mean distance is approximately 7 Å. For the final 20 ps, following the ring rotation, the distance has decreased to approximately 4.5 Å. Conversely, the mean distance between the *p*-NO_2 nitrogen and the $C_{\epsilon 2}$ atom of Trp-131 increases from approximately 3.5 Å to approximately 11.5 Å. At its closest approach, the *p*-NO_2 nitrogen of the simulated SSL-DNPhAETP is within 3.5 Å of (i.e., the nitro group is in van der Waals contact with) the N_ζ atom of Lys-681. This proximity offers a likely explanation for the labeling of Lys-681, instead of Trp-131.

Steric constraints in the docking of SSL-DNPhAETP required that the docked spiro ring point out of the active site, toward the solvent. More detailed analysis of the intermediate structures in the simulation shows that the new conformation with a rotated phenyl ring arises to alleviate steric overlap

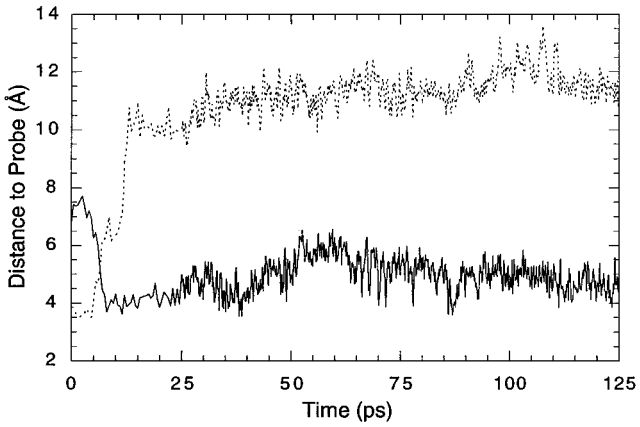

FIGURE 13: Distance as a function of time during the MD simulation between the *p*-NO_2 nitrogen on the phenyl ring of SSL-DNPhAETP and the N_ζ atom of Lys-681 (—) or the $C_{\epsilon 2}$ atom of Trp-131 (- - -).

between the phenyl ring and the spin probe moiety, which is present in the initial, crystal structure-like conformation. Trp-131 does not significantly change its location, continuing to point toward the open nucleotide pocket.

Two additional control simulations were carried out. In one, the initial position of the photoaffinity probe was taken as the time-averaged (2 ps) approximation of the final position of the SSL-DNPhAETP molecule following phenyl ring rotation. With this initial condition, the phenyl ring remained in its starting position close to Lys-681 during the entire subsequent 50 ps MD simulation, indicating that a stable equilibrium configuration had indeed been obtained. In another MD simulation, DNPhAETP (no spin probe moiety) was docked into the $S1_{sk}$ crystal structure using the orientation found in the MD_{dc}·DNPhAEDP·BeF_3 structure. In the absence of the added spin probe and attendant steric overlap, the phenyl ring did not rotate in the nucleotide pocket. It instead remained close to the crystal structure location, with the nitrogen of the *p*-NO_2 group pointing toward Trp-131. These simulations provide additional structural support for our conclusions as to why SSL-NANTP photolabels at Lys-681 while NANTP photolabels on the other side of the nucleotide pocket at Trp-131.

In summary, the interaction with rabbit fast skeletal muscle myosin S1 of a photoaffinity non-nucleoside ATP analogue having a spiro ring EPR spin-label, SSL-NANTP, has been described. This analogue is a substrate for myosin S1, and the diphosphate product is trapped stably at the active site using Vi and Ni^{2+}. The trapped analogue is photoincorporated into S1 at Lys-681 in the 20 kDa tryptic fragment with an approximately 14% yield. EPR spectroscopy indicates that the photoincorporated probe can bind in the myosin active site in a manner sterically analogous to that of SSL-NANDP that has not been covalently photoincorporated. Motion is restricted in a cone with a vertex angle of approximately 60°. After treatment with actin in the presence of MgATP, the ATPase rate of the photoincorporated S1−SSL-NANDP complex is remarkably similar to that of native S1 in the presence of Ca^{2+}, Mg^{2+}, or actin and Mg^{2+}, indicating that the photoincorporated probe can be displaced from the active site. The restricted motion of photoincorporated SSL-NANDP when bound in the active site suggests it as a useful probe of conformational changes at the active site during the motor cycle.

ACKNOWLEDGMENT

We are grateful to Dr. Gerhard Munske of the Washington State University Laboratory for Bioanalysis and Biotechnology for sequencing the peptides.

REFERENCES

1. Rayment, I., Rypniewski, W. R., Schmidt-Base, K., Smith, R., Tomchick, D. R., Benning, M. M., Winkelmann, D. A., Wesenberg, G., and Holden, H. M. (1993) *Science 261*, 50−57.
2. Fisher, A. J., Smith, C. A., Thoden, J., Smith, R., Sutoh, K., Holden, H. M., and Rayment, I. (1995) *Biochemistry 34*, 8960−8972.
3. Smith, C. A., and Rayment, I. (1996) *Biochemistry 35*, 5404−5417.
4. Gulick, A. M., Bauer, C. B., Thoden, J. B., and Rayment, I. (1997) *Biochemistry 36*, 11619−11628.
5. Dominguez, R., Freyzon, Y., Trybus, K. M., and Cohen, C. (1998) *Cell 94*, 559−571.
6. Houdusse, A., Kalabokis, V. N., Himmel, D., Szent-Gyorgyi, A. G., and Cohen, C. (1999) *Cell 97*, 459−470.
7. Gulick, A. M., Bauer, C. B., Thoden, J. B., Pate, E., Yount, R. G., and Rayment, I. (2000) *J. Biol. Chem. 275*, 398−408.
8. Kabsch, W., Mannherz, H. G., Suck, D., Pai, E. F., and Holmes, K. C. (1990) *Nature 347*, 37−44.
9. Holmes, K. C., Popp, D., Gebhard, W., and Kabsch, W. (1990) *Nature 347*, 44−49.
10. Rayment, I., Holden, H. M., Whittaker, M., Yohn, C. B., Lorenz, M., Holmes, K. C., and Milligan, R. A. (1993) *Science 261*, 58−65.
11. Schröder, R. R., Manstein, D. J., Jahn, W., Holden, H., Rayment, I., Holmes, K. C., Smith, C. A., and Rayment, I. (1993) *Nature 364*, 171−174.
12. Mendelson, R., and Morris, E. (1997) *Proc. Natl. Acad. Sci. U.S.A. 94*, 8533−8538.
13. Otterbein, L. R., Graceffa, P., and Dominguez, R. (2001) *Science 293*, 708−711.
14. Rayment, I., Smith, C., and Yount, R. G. (1996) *Annu. Rev. Phys. 58*, 671−702.
15. Yount, R. G., Lawson, D., and Rayment, I. (1995) *Biophys. J. 68*, 44S−47S.
16. Vale, R. D. (1996) *J. Cell Biol. 135*, 291−302.
17. Smith, C. A., and Rayment, I. (1996) *Biophys. J. 70*, 1590−1602.
18. Holmes, K. C. (1997) *Curr. Biol. 7*, R112−R118.
19. Cooke, R. (1997) *Physiol. Rev. 77*, 671−697.
20. Whittaker, M., Wilson-Kubalek, E. M., Smith, J. E., Faust, L., Milligan, R. A., and Sweeney, H. L. (1995) *Nature 378*, 748−751.
21. Jontes, J. D., Wilson-Kubalak, E. M., and Milligan, R. A. (1995) *Nature 378*, 751−753.
22. Irving, M., Allen, T. S., Sabidodavid, C., Craik, J. S., Brandmeier, B., Kendrick-Jones, J., Corrie, J. E. T., Trentham, D. R., and Goldman, Y. E. (1995) *Nature 375*, 688−691.
23. Corrie, J. E., Brandmeier, B. D., Ferguson, R. E., Trentham, D. R., Kendrick-Jones, J., Hopkins, S. C., van der Heide, U. A., Goldman, Y. E., Sabido-David, C., Dale, R. E., Criddle, S., and Irving, M. (1999) *Nature 400*, 425−430.
24. Sabido-David, C., Hopkins, S. C., Saraswat, L. D., Lowey, S., Goldman, Y. E., and Irving, M. (1998) *J. Mol. Biol. 279*, 387−402.
25. Xiao, M., Li, H., Snyder, G. E., Cooke, R., Yount, R. G., and Selvin, P. R. (1998) *Proc. Natl. Acad. Sci. U.S.A. 95*, 15309−15314.
26. Gollub, J., Cremo, C. R., and Cooke, R. (1996) *Nat. Struct. Biol. 3*, 796−802.
27. Baker, J. E., Brust-Mascher, I., Ramachandran, S., LaConte, L. E., and Thomas, D. D. (1998) *Proc. Natl. Acad. Sci. U.S.A. 95*, 2944−2949.
28. Pate, E., Nakamaye, K. L., Franks-Skiba, K., Cooke, R., and Yount, R. G. (1991) *Biophys. J. 59*, 598−605.
29. Wang, D., Pate, E., Cooke, R., and Yount, R. G. (1993) *J. Muscle Res. Cell Motil. 14*, 484−497.
30. Pate, E., Naber, N., Matsuka, M., Franks-Skiba, K., and Cooke, R. (1997) *Biochemistry 36*, 12155−12166.
31. Pate, E., Franks-Skiba, K., White, H., and Cooke, R. (1993) *J. Biol. Chem. 268*, 10046−10053.
32. Thomas, D. D. (1987) *Annu. Rev. Physiol. 46*, 691−709.
33. Crowder, M. S., and Cooke, R. (1987) *Biophys. J. 51*, 323−333.
34. Alessi, D. R., Corrie, J. E., Fajer, P. G., Ferenczi, M. A., Thomas, D. D., Trayer, I. P., and Trentham, D. R. (1992) *Biochemistry 31*, 8043−8054.
35. Wilson, G. J., Shull, S. E., Naber, N., and Cooke, R. (1997) *J. Biochem. 122*, 563−571.
36. Wang, D., Luo, Y., Cooke, R., Grammer, J., Pate, E., and Yount, R. G. (1999) *J. Muscle Res. Cell Motil. 20*, 743−753.
37. Chen, X., Grammer, J., Cooke, R., Pate, E., and Yount, R. G. (2000) *Bioconjugate Chem. 11*, 725−733.
38. Okamoto, Y., and Yount, R. G. (1985) *Proc. Natl. Acad. Sci. U.S.A. 82*, 1575−1579.
39. Wagner, P. D., and Yount, R. G. (1975) *Biochemistry 14*, 1900−1907.
40. Okamoto, Y., and Sekine, T. (1985) *J. Biochem. 98*, 1143−1145.
41. Grammer, J. C., Cremo, C. R., and Yount, R. G. (1988) *Biochemistry 27*, 8408−8415.
42. Pardee, J. D., and Spudich, J. A. (1982) *Methods Enzymol. 85*, 164−182.
43. Wells, J. A., Werber, M. M., Legg, J. I., and Yount, R. G. (1979) *Biochemistry 18*, 4793−4799.
44. Wagner, P. D., and Weeds, A. G. (1977) *J. Mol. Biol. 109*, 455−473.
45. Wells, J. A., Werber, M. M., and Yount, R. G. (1979) *Biochemistry 18*, 4800−4805.
46. White, H. D. (1982) *Methods Enzymol. 85*, 698−708.
47. Laemmli, U. K. (1970) *Nature 227*, 680−685.
48. Neville, D. C., Rozanas, C. R., Price, E. M., Gruis, D. B., Verkman, A. S., and Townsend, R. R. (1997) *Protein Sci. 6*, 2436−2445.
49. Pate, E., and Cooke, R. (1989) *Pfluegers Arch. 414*, 73−81.
50. Cope, M. J. T., Whisstock, J., Rayment, I., and Kendrick-Jones, J. (1996) *Structure 4*, 969−987.
51. Minehardt, T. J., Cooke, R., Pate, E., and Kollman, P. A. (2000) *Biophys. J. 80*, 1151−1168.
52. Grammer, J. C., Kuwayama, H., and Yount, R. G. (1993) *Biochemistry 32*, 5725−5732.
53. Weiner, S. J., Kollman, P. A., Nguyen, D. T., and Case, D. A. (1986) *J. Comput. Chem. 7*, 230−252.
54. Aqvist, J. (1992) *THEOCHEM 256*, 135−152.
55. Discover 2.9.7/95.0/3.0.0 User Guide (1999) Biosym/MSI, San Diego.
56. Goodno, C. C. (1979) *Proc. Natl. Acad. Sci. U.S.A. 76*, 2620−2624.
57. Phan, B., and Reisler, E. (1992) *Biochemistry 31*, 4787−4793.
58. Cole, D. G., and Yount, R. G. (1990) *J. Biol. Chem. 265*, 22537−22546.
59. Garabedian, T. E., and Yount, R. G. (1990) *J. Biol. Chem. 265*, 22547−22553.
60. Kerwin, B. A., and Yount, R. G. (1992) *Bioconjugate Chem. 3*, 328−336.
61. Werber, M. M., Peyser, Y. M., and Muhlrad, A. (1992) *Biochemistry 31*, 7190−7197.
62. Nakamaye, K. L., Wells, J. A., Bridenbaugh, R. L., Okamoto, Y., and Yount, R. G. (1985) *Biochemistry 24*, 5226−5235.
63. Luo, Y., Wang, D., Cremo, C. R., Pate, E., Cooke, R., and Yount, R. G. (1995) *Biochemistry 34*, 1978−1987.
64. Griffith, O. H., and Jost, P. C. (1976) in *Spin Labeling: Theory and Applications* (Berlinger, L. J., Ed.) Academic Press, New York.
65. Maruta, S., and Homma, K. (2000) *J. Biochem. 128*, 695−704.

BI0118411